Investigating Wind-Driven Rain Intrusion in Walls with the CARWASh

C.R. Boardman
Associate Member ASHRAE

Samuel V. Glass, PhD
Member ASHRAE

ABSTRACT

Wind-driven rain provides the primary external moisture load for exterior walls. Water absorption by the cladding, runoff, and penetration through the cladding or at details determine how a wall system performs. In this paper we describe a new laboratory facility that can create controlled outdoor and indoor conditions and use it to investigate the water management performance of a typical exterior wall assembly. Specifically we have quantified how much water gets past the cladding and hits the water-resistive barrier under particular conditions for a common lap siding.

The CARWASh (Chamber for Analytical Research on Wall Assemblies exposed to Simulated weather) was used to deliver wind-driven rain at two wind conditions and a range of rain intensities. The amount of wind-driven rain was measured on an exposed wall in the CARWASh. Results are presented as a function of wall location, wind speed, and rain intensity. Next, defects were introduced in the lap siding and absorbent pads were placed in the drainage cavity between the cladding and the sheathing to capture any moisture that got past the siding. Results are presented as a percentage of moisture getting past the cladding to incident wind-driven rain and are correlated with wind pressure across the cladding for various wind speeds and rain intensities.

INTRODUCTION

Wind-driven rain provides the primary external moisture load for exterior walls (Trechsel and Bomberg 2009; Straube and Burnett 2005). Hygrothermal and durability analysis of façades requires the quantification of the wind-driven rain loads (Blocken and Carmeliet 2004; Teasdale-St-Hilaire and Derome 2005). Software tools for transient hygrothermal analysis typically allow the user to specify a moisture source to represent wind-driven rain that intrudes past the cladding to simulate defects in construction and ensure a robust exterior wall system. ASHRAE Standard 160 (2009) provides criteria for inputs to transient hygrothermal models and includes a provision for rain penetration past the cladding, allowing a default value of 1% of the total wind-driven rain to get past the cladding, given limited measured data (Tenwolde 2011).

This study introduces a new laboratory facility that can create controlled outdoor and indoor conditions and thus help investigate the water management performance and moisture dynamics of exterior wall assemblies: the CARWASh (Chamber for Analytical Research on Wall Assemblies exposed to Simulated weather). One of the first uses for the CARWASh was to begin to supply measured data to better inform the modeling suggestion that 1% of wind-driven rain get past the cladding. The CARWASh was designed to provide realistic wind-driven rain under typical conditions. It is thus distinguished from other test facilities with different goals, such as the Wall of Wind, which is used to test under hurricane conditions (Bitsuamlak et al. 2009). It is further distinguished from spray tests, which rely on large pressure differences to force rapid water intrusion through wall defects (Sahal and Lacasse 2005). Spray rack and pressure systems are commonly used to test water penetration resistance for windows, with recent interest in dynamic pressure loading (Van Straaten et al. 2010; Lopez et al. 2011; ASTM 2011). While the CARWASh can apply modest pressure loads to a wall system, the primary intent was to use the force of the simulated wind to deliver

C.R. Boardman *is a general engineer and* ***Samuel Glass*** *is a research physical scientist at the Forest Products Laboratory, U.S. Forest Service, Madison, WI.*

Published by ASHRAE 2013

Figure 1 *Outside the CARWASh showing the wind blower.*

water to the wall from falling raindrops. The kinetic energy thus comes from the wind, and the dynamic wind pressure is the primary force moving water into wall defects.

This study reports on basic CARWASh capabilities, with a focus on the distribution of wind-driven rain on the exterior wall, and presents intrusion results from one cladding, a simple horizontal lap siding, with and without intentional defects. Future work will compare modeling and experimental results for newer wall systems and continue exploring wind-driven rain intrusion in other cladding systems.

MATERIALS AND METHODS

The CARWASh is a temperature- and humidity-controlled chamber large enough to mount a 10 × 10 ft (3.05 × 3.05 m) wall assembly between the inner and outer sections of the chamber; see Figure 1 for a photograph of part of the laboratory in which the CARWASh functions and Figure 2 for a schematic of the inside.

The small inner section (Figure 3) can simulate indoor conditions, ranging in humidity from 30%–70% relative humidity (RH) and temperatures (*T*) from 60°F to 80°F (15.5°C to 26.6°C). It also houses the measurement systems that can probe the wall for *T*, RH, and wood moisture content in various locations within an assembly, along with pressure differentials across wall assembly elements. The wall assembly can float on an air-cushioned platform that allows transport of a wall from the assembly area located near the CARWASh. The platform and wall fit into an opening between the two sections of the chamber, and any remaining gap is closed with an inflatable seal. Figure 4 shows a wall in place.

The larger outer section can simulate outdoor conditions, including wind, rain, and sun, ranging in dew point from 25°F to 80°F (–4°C to 27°C) and temperature from 30°F

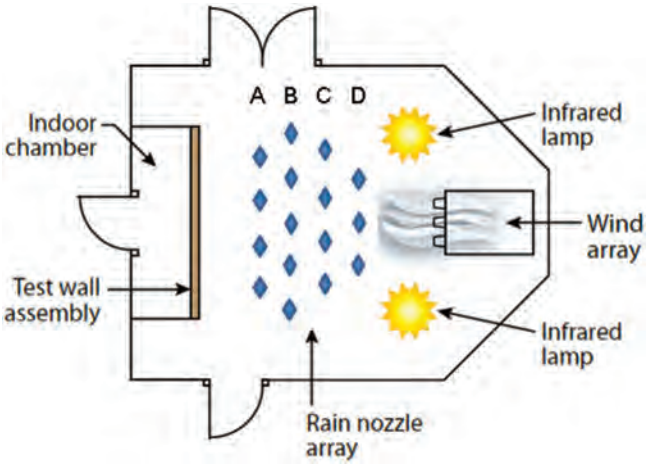

Figure 2 *Schematic of inside of CARWASh.*

to 110°F (–1°C to 43.3°C). Wind speeds range from 2 to 25 mph (1 to 11 m/s) supplied by a large blower that can oscillate in direction by 15° either side of center to produce changing wind speed and direction; see Figure 5 for a photograph of the wind array. Rain intensities range from 0.25 to 6 in./h (6 to 150 mm/h) supplied by four rows of nozzles (labeled A through D in the Figure 2 schematic) designed to produce realistic-sized raindrops. Three different nozzle sizes were used to achieve a smaller flow in the front and a larger flow in the back. The spray pattern is a wide-angle flat fan with uniform distribution and medium-sized drops, typical diameter near 0.03 in. (0.0007 m). The nozzles point straight down, intended to create a sheet of water drops that could be picked up by the wind so that the wind delivers the water to the wall. Each row can individually be turned on and off

Figure 3 *Small indoor chamber in CARWASh.*

Figure 4 *Wall installed between indoor and outdoor chambers, with wind and rain gauges.*

through computer control, and individual nozzles can be manually turned off if desired. Figure 6 shows a nozzle in action. The outer chamber also has infrared lamps (seen in Figure 5) that can simulate the drying effects of the sun, capable of heating from 0 to 100 W/ft^2 (0 to 1100 W/m^2). Return air ducts on each side of the wall assembly return air to the conditioning system for air recirculation, and grates in the floor return rainwater to a sump for water recirculation. By partially blocking the return air ducts a wind gust can be simulated. These gusts can last up to 5 s and apply an additional pressure up to 125 Pa (0.5 in. water).

Measuring Wind-Driven Rain

As a baseline for all work in the CARWASh we needed to characterize how much wind-driven rain was actually delivered to the wall under a variety of operating conditions. A number of wind-driven rain gauges were created out of polymethyl methacrylate (PMMA) with a collection area of 0.2 × 0.2 m (7.8 × 7.8 in.) following the recommendations of Blocken and Carmeliet (2006); see Figure 4 for one installed on a wall and Figure 7 for a close up of the latest design.

Captured rainwater was drained through the wall and collected in plastic containers that were weighed periodically. The CARWASh was set to operate at a variety of constant conditions so we could record the average rate of wind-driven rain deposited in each gauge. At any one time only four gauges

Figure 5 *CARWASh wind array, also showing IR heaters and rain spray nozzles overhead.*

Figure 6 *Rain nozzle in action inside CARWASh.*

were available, so the data was collected in five different runs and grouped into three sets of results. The first set of gauges (set I) was placed at mid-height of the wall, such that the bottom of the collector area was 50.25 in (1.27 m) from the top of the platform on which the wall sits; see Figure 8, Set I. Four gauges collected rain simultaneously, with the first positioned in the center of the wall such that the center of the collector area was 57.5 in. (1.46 m) from the left side as facing the wall. The remaining gauges were on the right side of the wall as shown in Figure 8, Set I. Set II was done with the four gauges in the center of the wall and extending down to allow us to study the effect of height, as shown in Figure 8, Set II. The lowest had its lowest collection level 22.25 in. (0.56 m) from the platform surface, with the others as shown in Figure 8, Set II. Set III explored wind-driven rain both left and right of center at a constant height of 30 in. (0.76 m) from the platform, as shown in Figure 8, Set III low, and at a height of 54.25 in. (1.38 m) across the full width of the wall, as shown in Figure 8, Set III high. The 4 gauges are numbered 2, 3, 6, and 7 in Figure 8, Set III low, to correspond to the same gauges when moved a bit higher in Figure 8, Set III high. Further, the final Set III high measurements were done in two runs (four gauges at a time) such that positions 4 and 5 are the same physical location in the center of the wall. Note also that Set III high included locations where defects were later introduced, namely at positions 1, 4, and 8.

The wind-driven rain data was analyzed using the theory from Straube and Burnett (2005) as outlined in their equation 12.1, but neglecting the angle between the wind and normal to the wall, since this is close to head-on in the CARWASh. Further, our Equation 1 assumes a core rain deposition factor (RDF) of 0.35 and introduces a location-specific factor (LF) that modifies the RDF to account for wind flow patterns at that location on the wall:

$$\mathrm{WDR} = \mathrm{LF} \times \mathrm{RDF} \times \mathrm{DRF} \times V \times r \qquad (1)$$

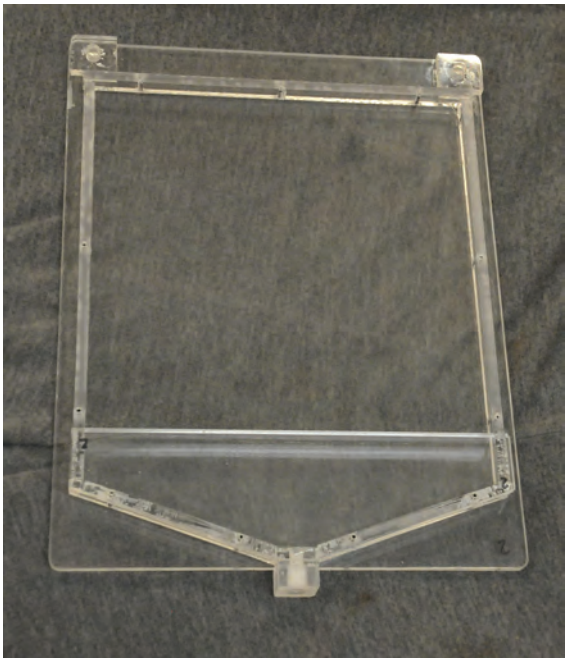

Figure 7 *Wind-driven rain gauge close up.*

Here WDR is the wind-driven rain at the surface location (kg/m^2·h), V is the velocity of the wind (m/s), and r is rain intensity on a horizontal surface (mm/h). The driving rain factor, DRF, accounts for the speed of falling raindrops,[1] which depends on the rain intensity and is calculated using Straube and Burnett's equation 12.2 in our Equation 2:

$$DRF = 0.22 \times r^{-0.123} \qquad (2)$$

In this analysis, the key is the LF, which should be near 1 if the RDF is actually 0.35. Of course the RDF in real buildings ranges widely depending on wind flow patterns, so we expect the LF to show divergence from our base case in the CARWASh.

Defects in the Siding and Measurement of Water Intrusion

The simple wall used for baseline wind-driven rain and intrusion measurements was an 8 in. (0.2 m) wide lap siding installed over a vertical strapping to form a rain screen. Generally there was 2 in. (0.05 m) of overlap, leaving a 6 in. (0.15 m) reveal. The strapping was attached to 7/16 in. (11 mm) oriented strand board sheathing on nominal 2 × 8 in. (38 × 184 mm) framing 16 in. (0.4 m) on center. Access panels were created, generally 11.75 × 18.75 in. (0.3 × 0.47 m), allowing absorbent pads to be placed on the outside of the sheathing (facing the siding, inside the rain screen gap). Four of these panels were used to detect any water getting past the siding by measuring

1. The units work out for Equation 1 because DRF has units of inverse velocity (m/s)$^{-1}$ and a rain intensity of 1 mm over a 1 m^2 surface yields 1 L of water, which weighs 1 kg.

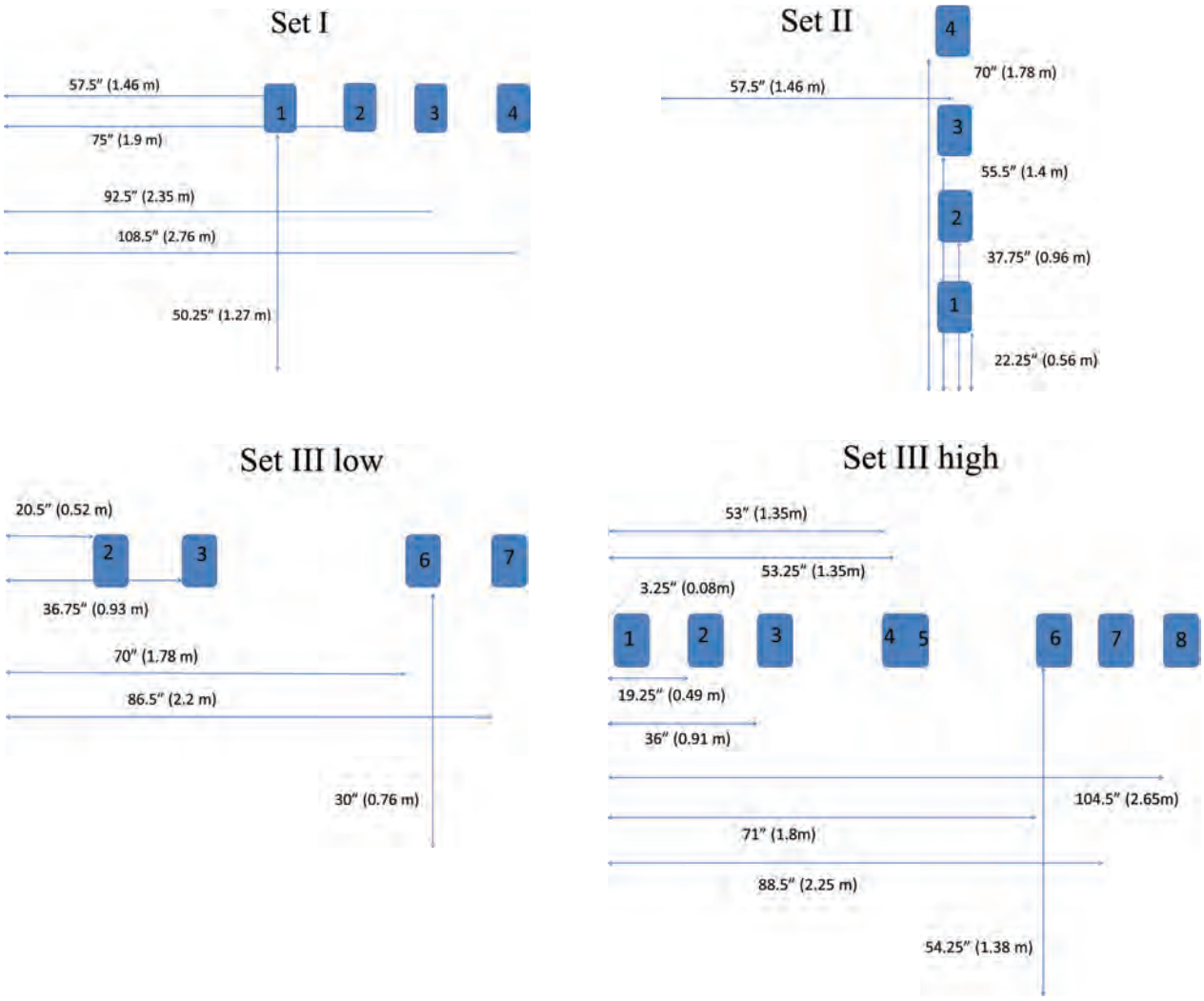

Figure 8 *Positions of wind-driven rain gauges.*

weight gain after a rain event. Two of the access panels were located at the edges of the wall, at middle height, with the bottom of panel 54 in. (1.37 m) from the platform and the outermost edge of the panel 4 in. (0.1 m) from the wall edge. The two middle panels were centered on the wall (again center of panel was 57 in. [1.44 m] from the left side), one at the same middle height as the other side panels and one just below it. The access panel locations can be visualized using Figure 8, Set III high, as capturing water entering at locations 1, 4, and 8, where the defects (described in the following paragraph) were introduced, and just below location 4, where there was no defect.

Defects in the siding were introduced by sliding a wedge up between the lap siding, creating a small, irregularly shaped gap (see Figure 9). Three of these defects were introduced at locations corresponding to the center of the access panels behind them, one at each of the two edges and one in the center, all at middle height such that the wedges were 61 in. (1.55 m) up from the platform. The gap thus created was largest in the center, from 0.177 to 0.24 in. (4.5 to 6 mm) tapering down to approximately a 0.118 in. (3 mm) gap when 7 in. (0.18 m) away from the center on either side. Under pressure from wind-driven rain, these gaps did allow water into the drainage cavity to be captured by the absorbent pads on the sheathing behind them.

Pressure Monitoring across the Siding

A number of experiments were performed to measure pressure differences across elements of the wall assembly at a variety of wind speeds. The differential pressure sensors could resolve pressure differences to 0.1 Pa (0.0004 in. water), and data acquisition was done at 20 Hz. Results are presented showing measurements directly across the cladding (see Figure 10).

RESULTS

Overall the wind-driven rain that falls on a particular location of a wall in the CARWASh depends on a large number of factors and is not simple to characterize. This reflects the

Figure 9 *Wedge to create defect in lap siding.*

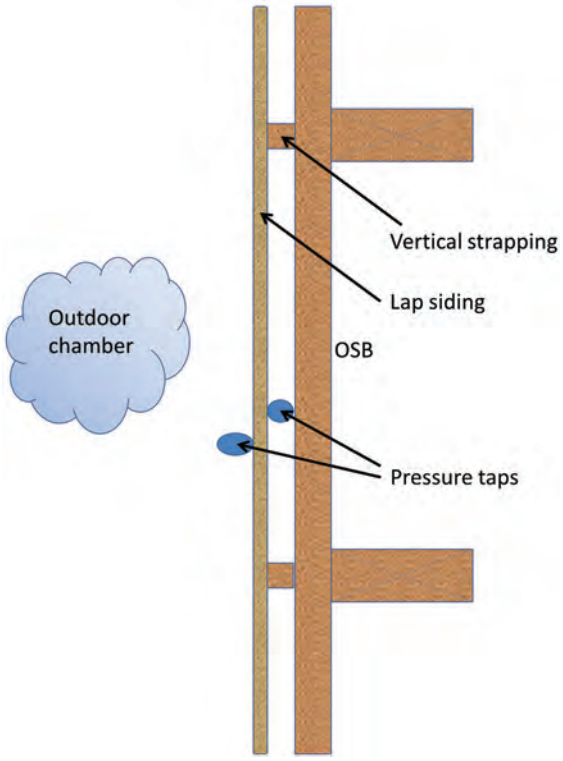

Figure 10 *Wall schematic with pressure taps across the cladding.*

complex fluid dynamics that control the wind flow and rain distribution and is approximated by Straube and Burnett (2005) in the RDF. We decided to limit the wind speeds investigated to 12 and 20 mph (5.3 and 8.9 m/s) to reduce the problem complexity. This reflects our rough observation that two wind flow patterns occur in the CARWASh. In the high-velocity case there is a more uniform pattern of wind-driven rain deposition on the wall and on other locations inside the chamber. However, the rain intensity is also a factor since it corresponds to which row of nozzles is turned on. For low-intensity rain events the front rows (A to B, front to back in Figure 2) are turned on, while for high-intensity rain events all the rows get turned on, with the back rows (C and D, furthest from the wall) providing more water. A further complicating factor is the ability of the CARWASh to shift the wind direction by sweeping the wind nozzle back and forth across the face of the wall by ±15°. To provide more realistic simulation of outdoor wind conditions we typically allowed this oscillation to vary the wind direction and arbitrarily set the oscillation period to 20 s. The wind-driven rain results shown in the following sections are average collection rates over sample periods greater than one hour so the wind direction differences are all averaged out.

WDR Set I—Locations Center to Right at Mid-Height

Table 1 presents the measured wind-driven rain (in kg/m^2·h) at the four locations for the first set of measurements investigating variation from center (WDR1) to the right side of the wall (WDR4) at mid-height. Table 2 helps interpret this data by providing the LF for each location when optimized over all the data to predict the WDR (first row), and when optimized only over similar wind speed and rain nozzle rows activated.

Inspection of Table 2 shows that the high-speed wind flow pattern provides more uniform distribution across the wall surface. To see this, first notice that LF4, the location to the far right, receives less wind-driven rain, as would be expected because the wind is less often blowing in that direction due to the blower oscillation. But also note that LF4 drops off more sharply for the low-speed conditions, indicating the less uniform distribution. Further, in the case with just row A where very little water is available, the high-speed case delivers less water to the wall because water is spread to other locations in the chamber. Finally, inspection of Table 2 also shows that our choice for overall RDF was reasonable, since the LF factors are close to 1.

WDR Set II—Locations in Center of Wall from Bottom to Mid-Height

Table 3 presents the measured wind-driven rain (in kg/m^2·h) at the four locations for the second set of measurements investigating variation from bottom (WDR1) to mid-height on the wall (WDR4) in the center. Table 4 helps interpret this data by providing the LF for each location when optimized over all the data to predict the wind-driven rain (first row) and when optimized only over similar wind speeds and rain nozzle rows activated.

Table 1. WDR: Mid-Height Center to Right —Set I

WDR1	WDR2	WDR3	WDR4	*V*, mph	*r*, in./h	Rows
9.0	8.2	5.2	2.4	12	1/2	A
8.7	8.1	5.5	2.7	12	1/2	A
9.5	9.2	6.1	3.6	20	1/2	A
10.8	10.0	6.9	4.1	12	3/4	A
13.3	11.8	8.1	5.1	12	1	A
6.2	6.3	6.1	5.5	20	1	A
11.8	9.7	6.2	2.8	12	3/2	A-B
22.6	20.7	19.8	15.8	20	3/2	A-B
25.3	27.7	25.1	18.3	20	2	A-B
25.5	27.7	25.4	18.4	25	2	A-B
28.7	24.5	18.9	9.2	15	3	A-C
11.2	9.5	8.7	6.5	5	4	A-C
25.4	27.3	23.6	11.6	10	4	A-C
41.3	42.2	37.4	18.5	15	4	A-C
54.4	56.9	53.6	38.7	20	4	A-C
54.8	57.0	53.5	37.9	20	4	A-C
59.6	61.5	57.5	39.4	20	4	A-C
56.1	59.0	50.4	35.7	25	4	A-C
67.4	68.8	66.0	40.5	20	5	A-D
85.0	90.1	81.9	55.4	25	6	A-D
76.8	80.8	74.6	49.4	25	6	A-D
28.0	31.7	26.0	12.0	12	6	A-D

Table 2. LF: Mid-Height Center to Right —Set I

LF1	LF2	LF3	LF4	Case
1.217	1.267	1.152	0.760	Overall fit
2.023	1.834	1.243	0.715	A low speed
0.743	0.745	0.618	0.490	A high speed
1.094	1.149	1.057	0.785	A-B all speed
1.314	1.288	1.102	0.553	A-C low speed
1.322	1.378	1.259	0.888	A-C high speed
1.193	1.250	1.157	0.760	A-D high speed
0.825	0.936	0.767	0.354	A-D low speed

Table 3. WDR: Center from Bottom to Mid-Height —Set II

WDR1	WDR2	WDR3	WDR4	*V*, mph	*r*, in./h	Rows
16.6	9.6	7.7	4.3	12	1/2	A
26.2	13.6	15.8	16.4	12	1	A
28.3	14.6	15.6	16.5	12	1	A
8.1	5.0	7.9	12.6	20	1	A
42.4	25.3	18.5	11.1	12	2	A-B
51.7	40.3	30.3	21.0	12	3	A-B
32.4	28.3	27.2	21.3	20	2	A-B
38.3	34.4	41.3	39.3	20	3	A-B
41.7	29.7	18.2	6.6	12	3	A-C
63.4	47.3	32.4	15.1	12	4	A-C
57.7	47.9	43.6	25.5	20	3	A-C
66.3	60.1	59.9	42.6	20	4	A-C
67.8	60.5	59.5	42.2	20	4	A-C
53.8	36.1	17.4	4.5	12	5	A-D
67.1	45.6	27.8	9.1	12	6	A-D
85.9	75.7	63.0	29.4	20	5	A-D
97.0	87.8	78.8	38.7	20	6	A-D
28.6	18.4	7.9	1.4	12	4	B-D
33.5	19.3	7.8	1.5	12	4	A-D

Table 4. LF: Center from Bottom to Mid-Height —Set II

LF1	LF2	LF3	LF4	Case
1.786	1.460	1.233	0.717	Overall fit
3.927	2.065	2.195	2.177	A low speed
0.688	0.424	0.674	1.075	A high speed
2.958	2.107	1.571	1.046	A-B low speed
1.759	1.426	1.383	1.146	A-B high speed
2.513	1.847	1.221	0.531	A-C low speed
1.734	1.530	1.486	1.014	A-C high speed
1.744	1.561	1.357	0.653	A-D high speed
1.929	1.305	0.728	0.221	A-D low speed

Table 5. Summary LF: Full Width at Two Heights —Set III

LF1	LF2	LF3	LF4	LF5	LF6	LF7	LF8	Height
1.014	1.438	1.364	1.224	1.232	1.277	1.154	0.768	54.25 in.
	1.261	1.268			1.126	1.021		30 in.

Inspection of Table 4 again confirms that high-speed flows show more uniform distribution, but there is more variation from bottom to top than from center to side, with the lower sections of wall generally receiving more wind-driven rain.

WDR Set III—Left and Right Asymmetry

Finally, a series of experiments at two different heights across the full width of the wall, measurement set III, showed that the wind-driven rain distribution was not as symmetric as expected, with the left side getting slightly more rain. This is illustrated in Table 5, which shows the overall summary fit LF (over all wind speeds and rain intensities) for each location. The top row corresponds to the height 54.25 in. (1.38 m) above the platform, with positions shown in Figure 8, Set III high. The second row of Table 5 corresponds to the height 30 in. (0.76 m) above the platform, with distribution as shown in Figure 8, Set III low.

Defects and High Wind Required for Rain Intrusion

Regardless of the wind speed or rain intensity, we never measured any rain intrusion past well-installed lap siding. The typical test was 20 mph (8.9 m/s) wind and 4 in./h (102 mm/h) rain intensity. One such test lasted 23 h with no weight gain in the absorbent pads. However, a similar near 8 h test with the gaps created by wedges at three locations did show intrusion. The amounts collected were very small, with 6.9 g (0.21 oz) at location 1 on the left side of the wall, 2.8 g (0.098 oz) at location 2 in the center of the wall, 2.8 g again at location 3 on the right, and 0 at location 4 just below location 2 but with no gap in the siding. These results are compared to a similar test done at 12 mph (5.3 m/s) wind speed and 2 in./h (51 mm/h) rain intensity in Table 6. That table shows the percent intrusion (intrusion ÷ incident of wind-driven rain × 100%) for the four locations. To area normalize the intrusion, each defect was assumed to represent a 6 × 11 in. (0.043 m^2) area corresponding to the revealed height of the lap siding and the width of the absorbent pad capturing the water behind the defect.

We are near the intrusion detection limit (around 0.05 g (0.002 oz) mass gain in the pad) with this method in the 12 mph test, with hardly any water getting past the siding, even with the defects. The wind speed appears to be the major factor allowing intrusion. Three more tests, all at rain intensity of 4 in./h but with increasing wind speeds of 12, 16, and 18 mph (5.3, 7.1, and 8 m/s), show this effect in Table 7. The only significant water intrusion (greater than 1 g [0.035 oz] of water in the pad) starts at 18 mph (8 m/s).

Table 6. Percent Intrusion—Four Locations

1	2	3	4	Case
0.046	0.015	0.026	0.000	4 in./h, 20 mph
0.001	0.000	0.001	0.000	2 in./h, 12 mph

Table 7. Percent Intrusion—Wind Speed Effects

1	2	3	4	Case
0.000	0.000	0.000	0.000	12 mph
0.001	0.000	0.001	0.000	16 mph
0.005	0.002	0.002	0.000	18 mph
0.046	0.015	0.026	0.000	20 mph

Pressure Measurements across the Cladding

Figure 11 shows a graph of pressure differential across the cladding (as in Figure 10) at two locations, near the defects, one in the center and one on the left side. These pressures are from 18 mph winds where we start to see rain intrusion, and they show peaks over 40 Pa (0.16 in. water) when the wind is blowing toward the left side of the wall.

The maximum pressure near 40 Pa at a wind speed of 18 mph is in the range we would expect from the stagnation pressure formula from Bernoulli's equation; see Equation 3 and Table 8.

$$P = \frac{\rho}{2} \times V^2 \qquad (3)$$

Note that the wind speeds reported were measured less than 3 ft (0.9 m) from the wall, 11 ft (3.3 m) from the nozzle, so they should be close to the wind speed normal to the wall just before it changes direction to flow along the wall surface. Further, most of the total pressure drop occurs across the cladding. Figure 12 compares the pressure drop across the whole assembly (i.e., from the outdoor chamber to the indoor chamber), with the drop only across the sheathing (the only resistance left after the cladding), for a wind speed of 20 mph, with the pressure taps on the left side of the wall.

It is not entirely clear why most of the drop is across the cladding. The access holes in the oriented strand board sheath-

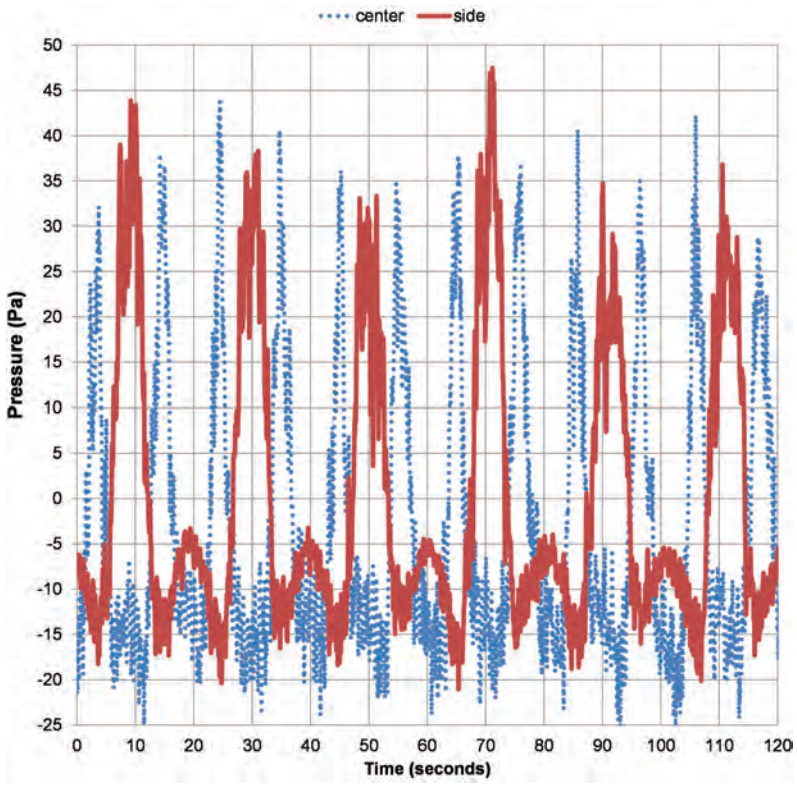

Figure 11 *Differential pressure across cladding at 18 mph.*

Table 8. Stagnation Pressure for Various Wind Speeds

P, Pa	*V*, mph
17.1	12
30.4	16
38.5	18
47.6	20

ing were gasketed, but there was no air barrier installed. Meanwhile, the cladding was fairly tight because the sides of the cladding were well sealed to keep out rain and the gaps at the top and bottom of the rain screen cavity were covered with metal flashing. Finally, in Figure 13 we can see the full range of the pressure variation across the cladding by comparing 12 and 20 mph pressure differentials in the center of the wall.

The maximum pressure values in Figure 13 again compare well with the stagnation pressures for the relevant wind speeds in Table 8.

DISCUSSION

In order to make further progress on specifying what percentage of water gets past the cladding we need to study more cladding types, and perhaps more importantly get a better handle on the kind of defects we expect. For example,

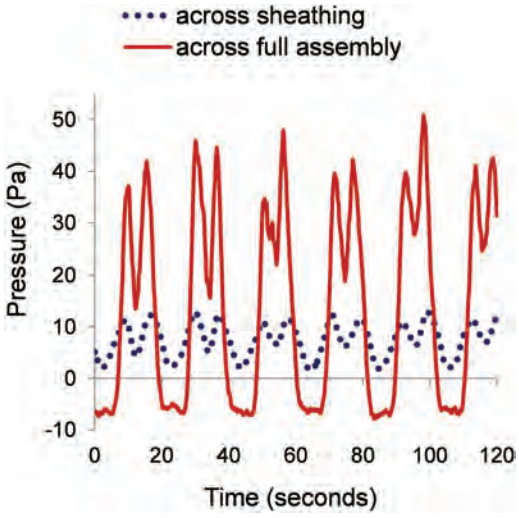

Figure 12 *Wind pressure for 20 mph across the full wall assembly was much greater than across only the sheathing.*

much larger amounts were measured by Sahal and Lacasse (2005). They worked with hardboard siding similar to our lap siding but introduced a number of defects, the most relevant of which was a penetration for a ventilation duct that was imperfectly flashed both at the cladding and at the sheathing. These defects allowed water to flow directly into the wall cavity.

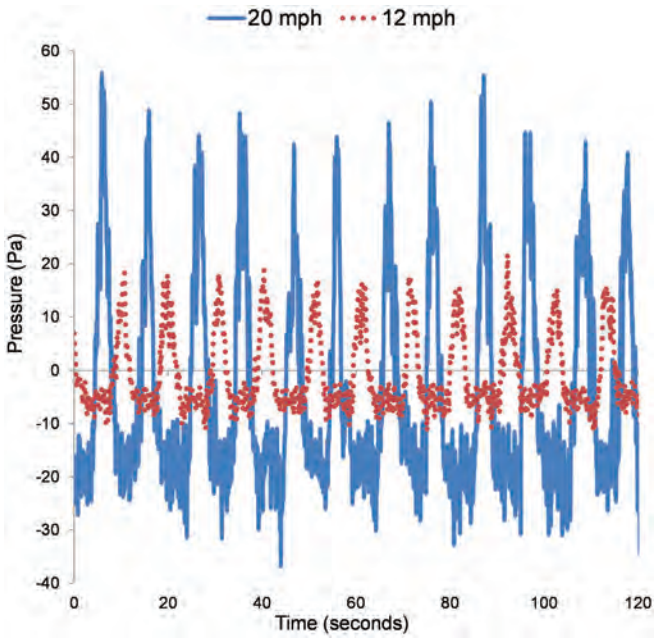

Figure 13 *Pressure across the cladding at two wind speeds.*

Sahal and Lacasse created a water entry function that relates the water intrusion at one defect, Q, with the spray rate (R_p, similar to the WDR) and a water entry potential, m_p, which depends on the pressure difference across the assembly. Their improperly flashed duct defect allowed 1000 times more water intrusion than our simple wedge that created a small gap in the lap siding. It may be helpful to follow an example calculation in which we produce an equivalent water entry potential for our defect.

Sahal and Lacasse (2005) define the water entry function:

$$Q = m_p \times R_p \quad (4)$$

where Q is the water entry rate (kg/min) and R_p is the spray rate (kg/min·m^2). For an example pressure difference of 50 Pa (0.2 in. water), their water entry potential, m_p, has a value of 1.3×10^{-2} (kg· min^{-1}/kg·min^{-1}·m^{-2}). This 50 Pa pressure roughly corresponds to our 20 mph wind speed, so we can use the 20 mph wind (8.9 m/s, 32.2 km/h) and 4 in./h (102 mm/h) rain intensity example to find in Table 6 that the average intrusion at a defect is near 0.03%. From Table 5 we see the typical LF is 1.2, so we can calculate the WDR from Equation 1 as about 48 kg/m^2·h, which we can convert to a spray rate R_p of 0.8 kg/min·m^2. Our Q, calculated as 0.03% of 0.8 kg·min^{-1}·m^{-2} times the area of 0.043 m^2, is 1×10^{-5} kg/min. Thus our mp value is 1.3×10^{-5}, or 1/1000 of the value of Sahal and Lacasse (2005).

This large difference in measured water intrusion from a defect reflects two different approaches to delivery of the water to the wall and different selections for the severity of defect. Sahal and Lacasse (2005) typically use large pressure differences, from 40 to 600 Pa, across the wall to drive water into the defect, and their spray rates (up to 300 kg/m^2·h) were typically higher than in the CARWASh, which had maximum wind-driven rain around 100 kg/m^2·h (3.9 in./h). We posit that the CARWASh conditions are closer to typical wind-driven rain patterns for most residential buildings. However, in this case the primary difference from our results is in the defect. Their defect fails to prevent water entry simply due to gravity. Even with no pressure difference across the wall, water cascading down the wall will enter their defects. Our defect requires wind-driven rain with a significant wind speed to see any intrusion.

An experimental setup and result similar to Sahal and Lacasse's (2005) can be seen in the window defect testing of Teasdale-St-Hilaire and Derome (2006). Acknowledging that high spray rate and large pressure differential tests represent extreme conditions, they used a WDR of 200 kg/m^2·h and pressure of 137 Pa to drive water into a window pane, where it cascaded down to small, 25 mm^2 area holes in the window-sill, representing defects in flashing. Each hole captured about 5% of the wind-driven rain, again about 1000 times the amount of water our defects saw. The window defects again allow water to run in by gravity.

Of course all wall systems should be designed to shed water cascading down the surface by gravity. If the façade allows water entry as if into a drain, and this water is not channeled back out through use of a secondary drainage plane, then modeling the wall system with 1% wind-driven rain getting past the cladding will not be enough. The local failures will be severe. However, if the wall defects are more like the gaps in our lap siding, then our first results hint that modeling 1% intrusion may be a bit high.

CONCLUSION

The general purposes for and capabilities of the CARWASh have been outlined. It can deliver realistic wind-driven rain to a full-size wall assembly, and we have presented details regarding the local distribution of that rain on the wall under different wind speeds and rain intensities. Details on rain intrusion into a particular kind of façade defect have been presented and contrasted with previous studies. Results suggest that we need to reflect further on the kinds of defects we intend to model and test with facilities such as the CARWASh.

ACKNOWLEDGMENTS

We acknowledge the support of the Forest Products Laboratory in carrying out this work. We thank Robert Munson for overall support and help in running the CARWASh. We benefitted from helpful reviews by Samuel Zelinka, Marshall Begel, and one anonymous reviewer.

NOMENCLATURE

LF = location factor; accounts for wind flow at location on wall, modifies RDF

RDF = rain deposition factor, fixed at 0.35 for our calculations but generally accounts for complex wind interactions with the wall

DRF = driving rain factor; accounts for speed of falling raindrops, m/s^{-1}

WDR = wind-driven rain, $kg/m^2 \cdot h$

V = wind velocity, m/s

r = rain intensity, mm/h

P = pressure, Pa

ρ = density, kg/m^3 (1.19 for air in Equation 3)

Q = water entry at a defect, kg/min

R_p = spray rate, similar to WDR, $kg/m^2 \cdot min$ (used in Equation 4)

m_p = water entry potential, m^2

REFERENCES

ASHRAE. 2009. ANSI/ASHRAE Standard 160, *Criteria for Moisture-Control Design Analysis in Buildings*. Atlanta: ASHRAE.

ASTM. 2011. ASTM Standard E2268, *Standard test method for water penetration of exterior windows, skylights, and doors by rapid pulsed air pressure difference*. West Conshohocken PA: ASTM International.

Bitsuamlak, G.T., A.G. Chowdhury, and D. Sambare. 2009. Application of a full-scale testing facility for assessing wind-driven-rain intrusion. *Building and Environment* 44:2430–2441.

Blocken, B., and J. Carmeliet. 2004. A review of wind-driven rain research in building science. *Journal of Wind Engineering and Industrial Aerodynamics* 92(13):1079–1130.

Blocken, B., and J. Carmeliet. 2006. On the accuracy of wind-driven rain measurements on buildings. *Building and Environment* 41:1798–1810.

Lopez, C., F.J. Masters, and S. Bolton. 2011. Water penetration resistance of residential window and wall systems subjected to steady and unsteady wind loading. *Building and Environment* 46:1329–42.

Sahal, N., and M. Lacasse. 2005. Water entry function of a hardboard siding-clad wood stud wall. *Building and Environment* 40:1479–91.

Straube, J.F., and E.F.P. Burnett. 2005. *Building Science for Building Enclosures*. Westford, MA: Building Science Press Inc.

Teasdale-St-Hilaire, A., and D. Derome. 2005. State-of-the-art review of simulated rain infiltration and environmental loading for large-scale building envelope testing. *ASHRAE Transactions* 111(2):389–401.

Teasdale-St-Hilaire, A., and D. Derome. 2006. Methodology and application of simulated wind-driven rain infiltration in building envelope experimental testing. *ASHRAE Transactions* 112(2):656–70.

Tenwolde, A. 2011. A review of ASHRAE Standard 160—Criteria for moisture control design analysis in buildings. *Journal of Testing and Evaluation* 39(1). DOI: 10.1520/JTE102896.

Trechsel, H.R., and M. Bomberg (eds). 2009. *Moisture control in Buildings: The Key Factor in Mold Prevention*, 2nd Ed. MNL 18. West Conshohocken, PA: ASTM International.

Van Straaten, R.A., G.A. Kopp, and J.F. Straube. 2010. Testing water penetration resistance of window systems exposed to "realistic" dynamic air pressures. *Proceedings of International Conference of Building Envelope Systems and Technology (ICBEST)*, Vancouver, June 27–30.